Volumetric relief map for the cortical subarachnoid space analysis

Alain Lebret, Yukiko Kenmochi, Jérôme Hodel, Alain Rahmouni, Philippe Decq, Eric Petit

HAL Id: hal-00926812

https://hal.archives-ouvertes.fr/hal-00926812

Submitted on 10 Jan 2014

Volumetric relief map for the cortical subarachnoid space analysis

Alain Lebret[a], Yukiko Kenmochi[b], Jérôme Hodel[c], Alain Rahmouni[d], Philippe Decq[e], Éric Petit[a]

[a]*Université Paris-Est, LISSI (EA 3956), UPEC, F-94010, Créteil, France*
[b]*Université Paris-Est, LIGM, UMR CNRS 8049, UPEM, F-77454, Marne-la-Vallée, France*
[c]*Hôpital Saint-Joseph, 185 Rue Raymond Losserand, F-75014, Paris, France*
[d]*Hôpital Henri Mondor, 51 Av du Maréchal de Lattre de Tassigny, F-94010, Créteil, France*
[e]*Hôpital Beaujon, 100 Bd du Maréchal Leclerc, F-92110, Clichy, France*

Abstract

Purpose   Medical image visualization is an important step in the medical diagnosis of hydrocephalus. In this paper, we present planar representations called volumetric relief maps that are generated from three-dimensional images of the cerebrospinal fluid within the cortical subarachnoid space. Such maps are visually interpreted at once and allow to automatically characterize fluid distributions. Consequently, they help specialists to provide a diagnosis and to monitor patients instantly.
Methods   Volumetric relief maps are generated by enclosing the cortical subarachnoid space with a hemisphere, and using a ray tracing method and a map projection technique from a hemisphere to a plane.
Results   Visualization of maps indicates that healthy adults have more balanced fluid distributions with well-filled sulci, unlike hydrocephalus patients who have more or less large fluid depletions in the posterior regions of the brain. We showed that a moment-based approach allows to efficiently characterize such fluid distributions from maps. In particular, the center of mass of a distribution is an efficient discriminant factor to distinguish between healthy adults and hydrocephalus patients, with resulting sensitivity and specificity of 100%. In addition, we have noted that asymmetry of the fluid distribution increases with depletion for hydrocephalus patients; such asymmetry is generally oriented towards the frontal part of the *fissura longitudinalis cerebri*.
Conclusions   This paper describes an innovative visualization tool used to analyze fluid distribution within the cortical subarachnoid space. It allows to efficiently discriminate between healthy adults and pathological cases, and to monitor patients before and after surgery.

Keywords: volumetric relief map, planar visualization, computer-aided diagnosis, patient monitoring, cerebrospinal fluid distribution, hydrocephalus

1. Introduction

Cerebrospinal fluid that is contained within the ventricles and subarachnoid space surrounds the central nervous system. The fluid circulates from ventricles where it is produced to the cortical subarachnoid space where it is resorbed into the circulatory system [1]. The importance of the cortical subarachnoid space has been highlighted in [2], especially in the case of hydrocephalus.

Hydrocephalus is a neurological pathology that usually results from an obstruction of the cerebrospinal fluid out-flow within the cerebral ventricles or subarachnoid space, and leads to several brain malfunctions. The most common test to diagnose hydrocephalus requires magnetic resonance imaging in order to identify the enlarged ventricles and any obstruction in the fluid pathway.

While three-dimensional images provide abundance of information, their interpretation and processing may be difficult and time-consuming. For example, analysis of cerebrospinal fluid spaces on magnetic resonance images
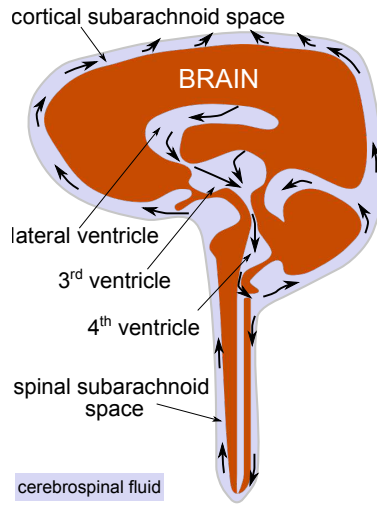

Figure 1: The cerebrospinal fluid circulates from ventricles where it is produced to the cortical subarachnoid space where it is resorbed.

requires from specialists to browse various slices according to different spatial planes, and occasionally using several magnetic resonance imaging sequences. As reported in [3], specialists generally have less time for analysis because they have to deal with a large amount of image datasets and more patients, which should necessitate more efficient and effective work environments. In order to help them perform effective diagnosis and patient monitoring, we propose a two-dimensional image representation, called volumetric relief map. Such a map can be visually interpreted with less difficulty and automatically processed faster, compared with its associated three-dimensional image. It immediately reports to specialists about the cerebrospinal fluid distribution within cortical subarachnoid space, and allows to estimate its variation compared with a reference value.

In order to generate such a map, the following three steps are mainly required: (1) setting an analytically defined surface (*e.g.* a hemisphere in this paper) that encloses the object to analyze, and (2) projecting some features of the object (*e.g.* its volume here) on the surface; (3) transforming automatically point positions on the surface into those on a plane. This new representation provides not only qualitative information on the object volume distribution (visually speaking) but also quantitative one (by using two-dimensional shape analysis techniques). For characterization of object volume distributions, we propose to perform a moment-based shape analysis, which will be routinely exploited and leads to functional parameters. We also show that these parameters are efficient to discriminate healthy adults from patients affected by communicating or non-communicating hydrocephalus, and to verify at a glance that the fluid distribution has returned to a "normal state" after a surgery.

This paper is organized as follows. In Section 2, we present some related work to our three-to-two-dimensional projection technique. Section 3 describes the method used to automatically generate a volumetric relief map from a three-dimensional image which highlights cerebrospinal fluid. In Section 4, we present relief maps produced from a clinical dataset of cortical cerebrospinal fluid volumes, and in Section 5 we analyze theses results using moment-based shape analysis techniques. Concluding remarks and perspectives are given in Section 6. This paper is an extended version of our previous paper [4], where more complete and detail information is given; for example, additional discussion on the robustness of the hemisphere positioning (see Section 3.1) and properties of volumetric relief map (see Section 3.4).

2. Related work

Production of a two-dimensional map from a three-dimensional object requires the following two ingredients: (1) an analytically defined surface that encloses the object to analyze and on which are projected some features; (2) a map projection technique from the surface to a plane.

2

Concerning the first ingredient, a sphere or an upper hemisphere is often used for brain analyses thanks to its shape similarity [5–8]. Features projected on a sphere or a hemisphere are, for example, gray values of the external cerebral cortex that are retrieved in [5] by using a ray casting technique [9, Chapter 13], while cortex surface curvatures or depths are projected by using a conformal map in [7, 8].

For the second ingredient, various methods have been studied for a sphere in cartography, *i.e.* for generating maps or representing the Earth on a flat surface (see [10] for a complete description of map projection techniques). In the medical field for example, an azimuthal equidistant projection has been applied in [5] for generating a "cartography" of the cerebral cortex surface. In fact, the azimuthal equidistant projection facilitates superposition on the map of data extracted from electroencephalography and magnetoencephalography measurements. Such a map is then used as an anatomical reference as all points on it are at proportionally correct distances and directions from the center point.

In this paper, we also use an upper hemisphere as enclosing surface, but we consider the volume of the object projected on surface points, instead of the gray value of the object [5] or the surface curvature or depth [6–8]. We then use a map projection technique that preserves areas, instead of distances, as it preserves the volume distribution information on the surface (see Section 3.3 for more details).

3. Methods

Suppose the cortical subarachnoid space is pre-segmented, for example, by using the method presented in [11], which is also outlined in Section 4.2. Given its volume data, *i.e.* a three-dimensional voxel set, its associated volumetric relief map is generated in the following two steps. In the first step, we consider an upper hemisphere which is automatically positioned, such that it encloses the superior part of the segmented cortical subarachnoid space. Every voxel is then projected on the hemisphere, so that the inside voxel distribution can be observed on the surface of the hemisphere. In the final step, we generate a two-dimensional image by projecting every point on the hemisphere onto a plane. Note that the chosen projection preserves a point distribution in a similar way between the original one on the hemisphere and the new one on the plane. The key point is that we preserve the total amount of fluid volume after the two projections above, and thus in the volumetric relief map. Each step is explained in details as follows. At the end, some properties of volumetric relief maps are also presented.

3.1. Automatic positioning of a hemisphere

The aim of the positioning is to prevent any rotation of the cortical subarachnoid space during image acquisition. First, the hemisphere center is positioned at the top rear of the cerebral aqueduct, which is a visible structure in the "fluid specific" magnetic resonance images used in the clinical dataset [12] and whose top rear position is closest to the posterior commissure. This latter contains the pineal gland, which is considered as the geometric center of the brain [13]. Thus, what we need is to locate the cerebral aqueduct automatically from an initial magnetic resonance image. The method presented in [11] and also summarized in Section 4.2 is specific to these particular images. Note that it allows us to automatically locate not only the cerebral aqueduct, but also the eyeballs, which will be used to set the anatomical reference axes below.

After setting the hemisphere center $\vec{c}$, its radius is calculated such that it is superior to the maximum distance from $\vec{c}$ to voxel points of the cerebrospinal fluid volume, as illustrated in Fig. 2.

Finally, the base of the hemisphere is set to match the plane that passes through the hemisphere center and the tops of the eyeball boundaries.

In order to generate a volumetric relief map, we additionally need two orthogonal axes crossing at the hemisphere center on its base, which will correspond to vertical and horizontal axes in a volumetric relief map. The vertical axis is then determined as the intersection between the hemispherical base plane and the bisector of the tops of the two eyeball boundaries. In practice, the bisector contains the *fissura longitudinalis cerebri* and the base corresponds to an axial plane, as illustrated in Fig. 2. Alternatively to this automatic positioning, certainly the manual setting by specialists is also possible for its refinement.

3.2. Voxel distribution on a hemisphere

Once we set the upper hemisphere as above, we generate a voxel distribution on it as follows. The main idea is that each voxel is considered to have the unit fluid volume, and this unit quantity is represented by the voxel center.
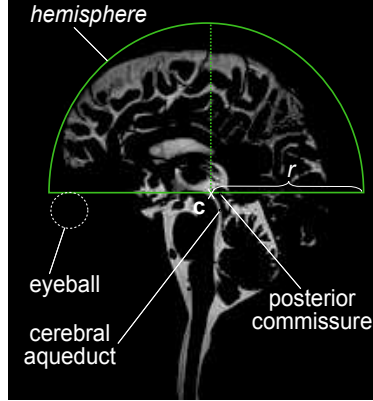
Figure 2: Positioning of the hemisphere of center $\vec{c}$ and radius r to cover the superior cortical subarachnoid space. Position of eyeballs is also indicated (with dashed circle).

With this consideration, the fluid distribution can be replaced by the voxel center distribution, so that we only need to project voxel centers to the hemisphere.

Let $\vec{c}$ be the center of the projection hemisphere and r be its radius. We project each voxel center point $\vec{v}$ to the hemisphere by drawing a three-dimensional ray [9, Chapter 14] starting at $\vec{c}$ and going in a direction $(\vec{v} - \vec{c})$ to obtain its intersection with the hemisphere. This intersection is the projected point of $\vec{v}$ on the hemisphere, denoted by $p(\vec{v})$, as illustrated in Fig. 3a. Note that different $\vec{v}$ can have the same projected points $p(\vec{v})$ if they are colinear.

3.3. Volumetric relief map as a two-dimensional image

All voxel-center points projected on the hemisphere, $p(\vec{v})$, are now mapped on a two-dimensional plane as illustrated in Fig. 3b. During this mapping, we intend to keep the fluid distribution information, *i.e.* the distribution of $p(\vec{v})$, as mentioned above. For this reason, the Lambert azimuthal equal-area projection is chosen as it has the following interesting properties: bijection, diffeomorphism, direction preservation from the point of tangency and area preservation [10, Chapter 3]. In particular, area preservation is essential since it indicates that we may be able to have the same number of projected points on the plane in a unit surface area as that of the original points on the hemisphere in a unit area. The Lambert projection preserves neither angle nor distance, and thus shapes can be distorted in the plane by moving away from the point of tangency. However, such distortion is less observed if the projection is restricted to the hemisphere centered at the point of tangency (*i.e.* the upper hemisphere in this paper) [14].

More concretely, the following formulas are applied for each point $p(\vec{v}) = (x, y, z)$ on the hemisphere, such that $(x - c_x)^2 + (y - c_y)^2 + (z - c_z)^2 = r^2$ and $z \geq c_z$, in order to obtain the two-dimensional point $P(\vec{v}) = (X, Y)$ in the disc with center at the origin and radius $\sqrt{2}r$:

$$X = \sqrt{\frac{2r}{r + z - c_z}}(x - c_x),$$

$$Y = \sqrt{\frac{2r}{r + z - c_z}}(y - c_y).$$

To generate a volumetric relief map which is a two-dimensional image, we digitize the disc obtained by the Lambert projection. Suppose that the disc is digitized with a square grid of pixel size $\sqrt{2}r/N$ by using the Gaussian digitization (*i.e.* a pixel is considered in the digitized disc if the center point is in the original disc) [15, Chapter 2]. The obtained two-dimensional image containing this digitized disc thus has the support of size $(N + 1) \times (N + 1)$ as illustrated in Fig. 3c.

For each voxel center $\mathbf{v}$, its projected point $\mathbf{P}(\mathbf{v})$ then votes for the pixel that contains $\mathbf{P}(\mathbf{v})$ itself as illustrated in Fig. 3d. The voting procedure associates each projected point to a single pixel. After this voting procedure for all projected points, we add up for each pixel the number of its associated voxels, *i.e.*, its associated fluid volume
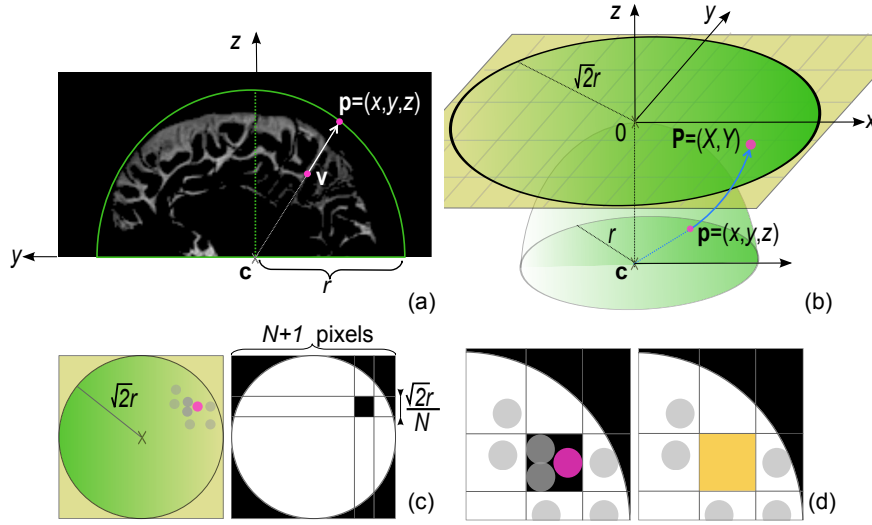
4

Figure 3: Steps of the geometric relief map generation: positioning the hemisphere of center $\vec{c}$ and radius r to cover the three-dimensional object (here the superior cortical subarachnoid space) and projecting each voxel $\vec{v}$ to its corresponding point $\vec{p}$ onto the hemisphere (a); mapping each $\vec{p}$ to its corresponding point $\vec{P}$ on the two-dimensional plane using the Lambert azimuthal equal-area projection (b); digitizing the disc in the two-dimensional grid $(N + 1) \times (N + 1)$ (c); voting each $\vec{P}$ for a pixel of the disc (d).

quantity. Each pixel value of a volumetric relief map corresponds to the amount of fluid between the chosen center of the cortical subarachnoid space, *i.e.*, the top rear of the cerebral aqueduct, and the associated point on the hemisphere. Briefly speaking, it gives an idea to approximate depths within the subarachnoid space, *e.g.*, depths of cerebral sulci.

3.4. Properties of volumetric relief map

A volumetric relief map has the following interesting properties:

Property 1. *Each voxel of a given voxel set is associated to exactly one pixel in the volumetric relief map.*

Property 2. *The total amount of pixel values in a volumetric relief map is equal to the total volume of the initial three-dimensional voxel set.*

Property 2 is straightforwardly obtained from Property 1, which is also directly induced by the voting procedure explained in Section 3.3.

Note that the volumetric relief map may be influenced by the two- or three-dimensional space digitizations. As a matter of fact, the Lambert equal-area projection helps every pixel to have a similar voxel quantity for a digitized solid-hemispherical object centered at (c_x, c_y, c_z) if we do not set N to be too large for the relief map size, with respect to the resolution of the original volumetric image.

Let us consider a digitized hemisphere with radius R (unit voxels), whose volume is thus $\frac{2}{3}\pi R^3$ (unit voxels). Suppose that we make a volumetric relief map with the same radius R (unit pixels, instead of unit voxels), then Property 2 leads us to the conclusion such that each pixel must be associated to $\frac{2}{3}R$ (unit voxels), as the digitized circle region on the volumetric relief map contains πR^2 (unit) pixels approximately. Figure 4 illustrates an example for a digitized hemisphere with radius $R = 40$, and its volumetric relief map whose values are around 26.7 almost everywhere in the digitized circle. In practice, digitization causes some variations of this value. However, such a digitization influence can be reduced in a volumetric relief map by applying a Gaussian filter with a small window to the map.

From this experience, the following observation can be made.

Observation 1. *The projections of voxel centers in a voxel space are uniformly distributed in the volumetric relief map, if the pixel size of the map is sufficiently large with respect to the voxel size.*
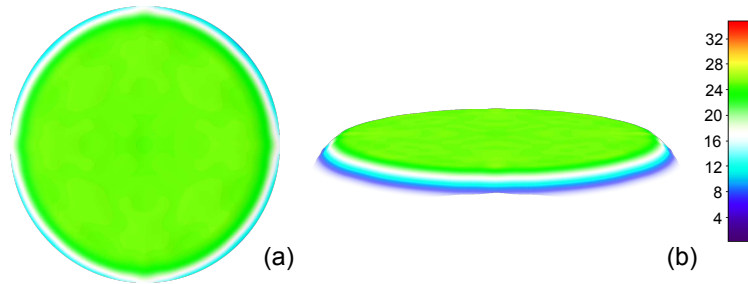
5

Figure 4: Volumetric relief map (with size 81×81) of a filled hemisphere with radius $R = 40$.

In practice, the pixel size of a volumetric relief map is set not to be excessively smaller than the voxel size of the original three-dimensional image. Otherwise, we will have empty pixels in a volumetric relief map, to which no voxel is associated due to the image digitization.

4. Experiments

This section describes experiments we have carried out. We generate volumetric relief maps in order to visualize cerebrospinal fluid distribution within the superior cortical subarachnoid space.

4.1. Clinical dataset

The clinical dataset is composed of 74 different subjects (median age: 48 years old; range: 18–91 year olds): 44 healthy volunteers and 30 patients with hydrocephalus, among which there are 25 communicating hydrocephalus and 5 non-communicating hydrocephalus. Moreover, eight of the patients had another image acquisitions after their surgery.

Magnetic resonance images of the intracranial cerebrospinal fluid were acquired in the sagittal plane on a 1.5 T system (Magnetom Avanto; Siemens Medical Solutions, Erlangen, Germany). The sequence used for the experiments is a variant of the T2-weighted turbo spin echo sequence with variable flip-angles called SPACE (Sampling Perfection with Application optimized Contrast using different flip-angle Evolution) which is a fluid specific sequence [12]. On these images, the cerebrospinal fluid appears as a homogeneous hypersignal as shown in Fig. 2 in order to facilitate the fluid segmentation. Sequence for the clinical image acquisition of intracranial cerebrospinal fluid was set as follows: repetition time TR (ms) / echo time TE (ms) of 2400 / 762; 141 turbo factor; 250×250 mm field of view; 256×256 acquisition matrix; 1 mm isotropic resolution; 1.4 for number of excitations; 160 slices; 3 min for acquisition time [12].

4.2. Automatic three-dimensional image pre-processing

The automatic three-dimensional image pre-processing step consists in segmentation of the cerebrospinal fluid volume from an initial image, followed by separation of ventricular and subarachnoid spaces. Here, we summarize the method presented in [11], which is specific for the type of magnetic resonance images explained above.

The first main step, namely segmentation of cerebrospinal fluid volume, is homotopically thickening an initial result, which is obtained by the moment-preserving thresholding method thanks to image (gray value) properties and set within the entire cerebrospinal fluid. A topological assumption on the fluid shape detailed in [11] is also used. This results in not only segmenting the cerebrospinal fluid volume but also both eyeballs, which are visible on initial images [11] and used in the next procedures as references (for example, positioning an hemisphere in Section 3.1).

Separation of ventricular and subarachnoid spaces requires to detect the cerebral aqueduct which is a specific vessel-like structure within the ventricular space. Detection of the aqueduct expects to locate eyeballs and uses a region of interest in order to restrict searching. The region of interest is automatically set from the eyeballs information mentioned above. The cerebral aqueduct enhancement is performed by a vessel segmentation filter using Hessian as proposed in [16] which allows to dissociate strict tubular structures from others. The filter is initialized with 5 scale spaces σ from 0.4 to 0.9, and its parameters α, β and c are set with values $\alpha = 0.7$, $\beta = 0.2$ and $c = 200$. As a result,
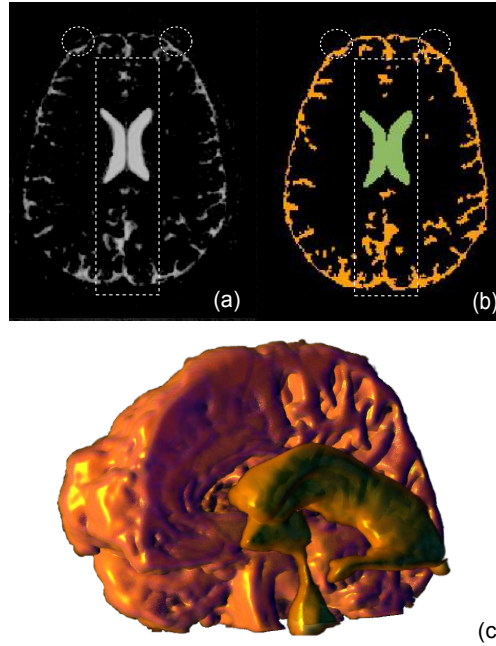
6

Figure 5: Three-dimensional image pre-processing, by setting a region of interest (illustrated as a dashed-line rectangle) based on the positions of eyeballs (in dashed circles), for separating ventricular and subarachnoid spaces: (a) an axial cross-section of an original image; (b) the cross-section of the segmented ventricular and cortical subarachnoid spaces, represented respectively in green and orange; (c) a partial three-dimensional surface rendering of the cortical cerebrospinal fluid (the subarachnoid space was cut along the midsagittal plane).

the cerebral aqueduct is found as the longest tubular structure with the highest intensity range in the most median sagittal planes within region of interest.

Finally, ventricles are recovered by a morphological geodesic reconstruction using a flat ball of radius $r_d = 1$ from the cerebral aqueduct chosen as a marker [17]. The geodesic reconstruction is restricted to the region of interest. It generates an image composed of regional maxima due to the threshold decomposition used in [17]. Then, the ventricular space is recovered using a h-dome transform [17] on the union of regional maxima whose intensities are greater than or equal to those which constitute the cerebral aqueduct.

Figure 5 shows the result of such an automatic separation between the ventricular space and the cortical subarachnoid one.

4.3. Map generation

After the pre-processing step, we applied to each pre-segmented image of the dataset the method presented in Section 3. The process to generate volumetric relief maps took place on a conventional computer (Intel Pentium Dual Core 2.70 GHz / 8 GB main memory, GNU/Linux 3.8 operating system), and an application software was implemented in the Java programming language using the image processing package Fiji [18].

Volumetric relief maps were initialized with a width of 203 pixels, which is not far from the maximum value determined depending on deviated sizes of the pre-segmented superior cortical subarachnoid spaces, and the radius of the hemisphere was set to 100 mm. The overall time of image acquisition including pre-processing and map generation is less than 4 min for each patient: 3 min for image acquisition, 50 seconds for pre-processing and 1 second or less for map generation.

Figure 6 shows a volumetric relief map example for a healthy volunteer. Note that the positioning of the hemisphere allows to fix the *fissura longitudinalis cerebri* with the vertical axis and the projection of the top rear of cerebral aqueduct with the map center.
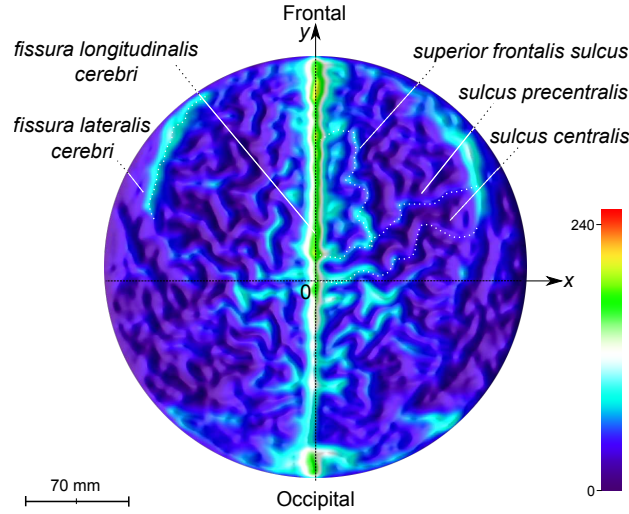
Figure 6: An example of colored volumetric relief map for a healthy adult. Note that the frontal region is on the upper part of the map and the occipital region is on the lower part. The *fissura longitudinalis cerebri* separates the map vertically and appears brighter.

5. Analysis of volumetric relief maps

In this section, we analyze the generated volumetric relief maps qualitatively and quantitatively, in order to understand the fluid distribution and its structure. For quantitative analysis, we apply a moment-based approach on those fluid distribution results, with a discriminant analysis, and also make some observations on monitoring of patients.

5.1. Visual analysis of volumetric relief maps

For almost every healthy adult, the fluid distribution is fairly distributed on the entire volumetric relief map with well-filled sulci as shown in Fig. 6. The *fissura longitudinalis cerebri* stretches over most of the height of the map with a high intensity, separating the map in two balanced regions. Furthermore, the *sulcus centralis* can be located closely to the horizontal axis and the *fissura lateralis cerebri* is visible near the frontal boundary of the map with a substantial intensity.

Volumetric relief map examples for communicating and non-communicating hydrocephalus patients are shown in Fig. 7. Clearly, we see different distributions from their corresponding volumetric relief maps. Both patients lose symmetry, but communicating hydrocephalus patient has less fluid within the *fissura longitudinalis cerebri* and the *fissura lateralis cerebri* in particular (Fig 7a), whereas non-communicating one has less fluid everywhere, in the center as well, except in the *fissura lateralis cerebri* (Fig. 7b).

Figure 8 shows the volumetric relief maps for one of the patients before (a) and after (b) his surgery. Before surgery, as observed from Fig. 8a, fluid depleted regions (black and dark blue colors) occur mainly on the lower part of the map and the fluid within *fissura longitudinalis cerebri* is reduced. Those depleted regions are related to the occipital lobe and posterior parts of both the temporal lobes and parietal ones. After surgery, as observed from Fig. 8b, the intensity within all cerebral sulci increased as cerebrospinal fluid has recovered its balanced distribution and depleted regions were almost restored. Note that in this particular case, the *fissura longitudinalis cerebri* does not seem to stretch yet to the entire height with a high intensity, but clearly elongates more than before.

Volumetric relief maps also allow us to effortlessly make an estimation of depths of cerebrospinal fluid within cerebral sulci, *i.e.* sulcal depths, by verifying depths of healthy adults. We reported the mean depth values of cerebrospinal fluid inside the main cerebral sulci related to the superior cortical subarachnoid space in Table 1. Those values are consistent with the recent results presented in [19, 20]. Furthermore, Fig. 9 shows profiles of the fluid depths along the medial axis [15, Chapter 3] of some sulci, manually retrieved from relief maps of the patient before and after surgery in Fig. 8. If we compare profiles before and after surgery, their difference provides the depletion
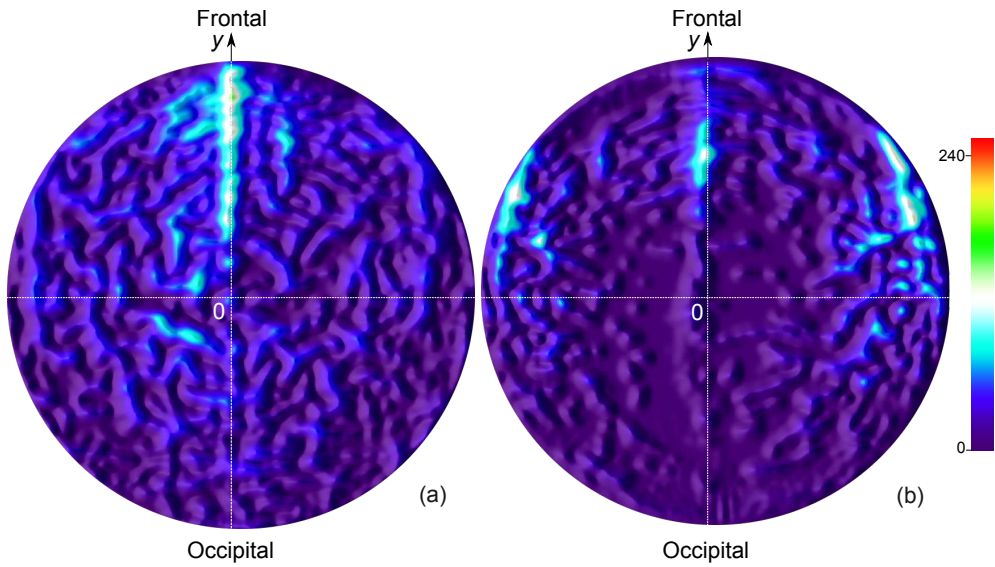
Figure 7: Colored volumetric relief maps for a communicating hydrocephalus patient (a) and a severe non-communicating one (b).
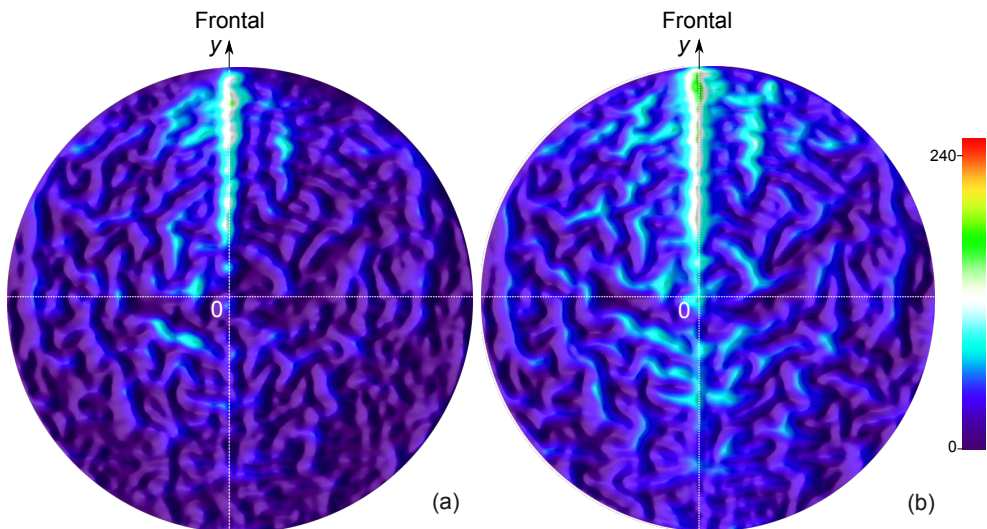

Figure 8: Colored volumetric relief maps for a communicating hydrocephalus patient before (a) and after (b) a surgery. Note that the depleted region (black and dark blue colors) in the lower part of the map in (a) is reduced in (b) and the *fissura longitudinalis cerebri* is less bright in (a) than (b). It is also observed that the fluid has recovered a more balanced distribution after surgery.

9

Table 1: Assessment of the cerebrospinal fluid depths in the main cerebral sulci related to the superior cortical subarachnoid space, along their medial axis. Each value is represented by (mean ± standard deviation).

Sulcus	Class	Depth of fluid (mm)
centralis	healthy	55.32 ± 14
	pathological	29.14 ± 15
precentralis	healthy	55.19 ± 16
	pathological	34.88 ± 9
postcentralis	healthy	63.88 ± 18
	pathological	35.13 ± 14
frontalis superior	healthy	58.12 ± 17
	pathological	44.95 ± 15
intraparietalis	healthy	57.28 ± 21
	pathological	26.01 ± 15

intensity inside a sulcus for a hydrocephalus patient. Note that such assessments require manually arduous tasks or complicated segmentation methods when three-dimensional images are directly used [20].

5.2. Moment-based analysis of the fluid distribution

In order to assist specialists to confirm their visual analysis of volumetric relief maps, we extract geometric characteristics of a fluid distribution from each map by using a moment-based approach presented in [21].

Quantitative assessments on the clinical dataset were carried out by calculating low order geometric moments for each volumetric relief map, *i.e.* the center of mass, principal axis and skewness coefficients. Results are summarized in Table 2.

First, the resulting distribution of centers of mass for healthy adults and pathological cases is shown in Fig. 10. Regarding the distribution, healthy adults have the average center of mass close to the relief map center. In contrast, every hydrocephalus patient has a fluid distribution more or less depleted in the posterior and lateral regions of the brain, with larger deviations around the *fissura longitudinalis cerebri* than healthy adults. This confirms the visual analysis, which indicates the decrease of cerebrospinal fluid inside sulci, as shown in Section 5.1. The relative change of the averages of centers of mass between healthy adults and patients is −80% along the vertical axis of the map.

Concerning distributions of principal axes for healthy adults and pathological cases, both of their averages are almost along the *fissura longitudinalis cerebri* and are oriented towards the frontal region; there are very few patients who have orientations differing from that of the *fissura longitudinalis cerebri*. This indicates that the principal axis, *i.e.* the fluid distribution orientation, may not be a relevant discriminant factor when volumetric relief maps are used. Compared to the principal axis of an original three-dimensional image, we may lose the depth information that is different between healthy adults and hydrocephalus patients (as discussed in Section 5.1). Indeed, healthy adults tend to have their major axes oriented towards the frontal regions parallel to an axial plane, while major axes of patients also tend to be oriented toward the frontal regions but slightly decline to their lower parts; it is obvious that this distinction is impossible when volumetric relief maps are used.

Finally, the skewness coefficients exhibit that the fluid distribution has a low degree of deviation from symmetry about the center of mass for a healthy adult. On the other hand, hydrocephalus patients have moderate asymmetry towards the frontal region of the *fissura longitudinalis cerebri*, indicated by negative skewness coefficients Sk_y. Differently from Sk_y, Sk_x varies in signs. Furthermore, the sign of Sk_x seems to depend on the sign of C_x of the center of mass (C_x, C_y); $Sk_x < 0$ if $C_x > 0$ and $Sk_x > 0$ if $C_x < 0$. In fact, Fig. 11 illustrates that the absolute value of each skewness coefficient increases with respect to the distance from the center of mass to the average center of mass of healthy adults. Let d be the distance from each center of mass (C_x, C_y) to the average center of mass of healthy adults. Given a set of the skewness coefficients Sk_x and Sk_y, as well as a set of associated distances d, we make polynomial regression which fits a nonlinear model to them. This results in the following quadratic models using an ordinary least squares method [22]:

$$\begin{cases} Sk_x &= -0.0113d + 0.0002d^2 \quad \text{if } C_x > 0, \\ Sk_x &= 0.0134d - 0.0002d^2 \quad \text{otherwise,} \end{cases}$$
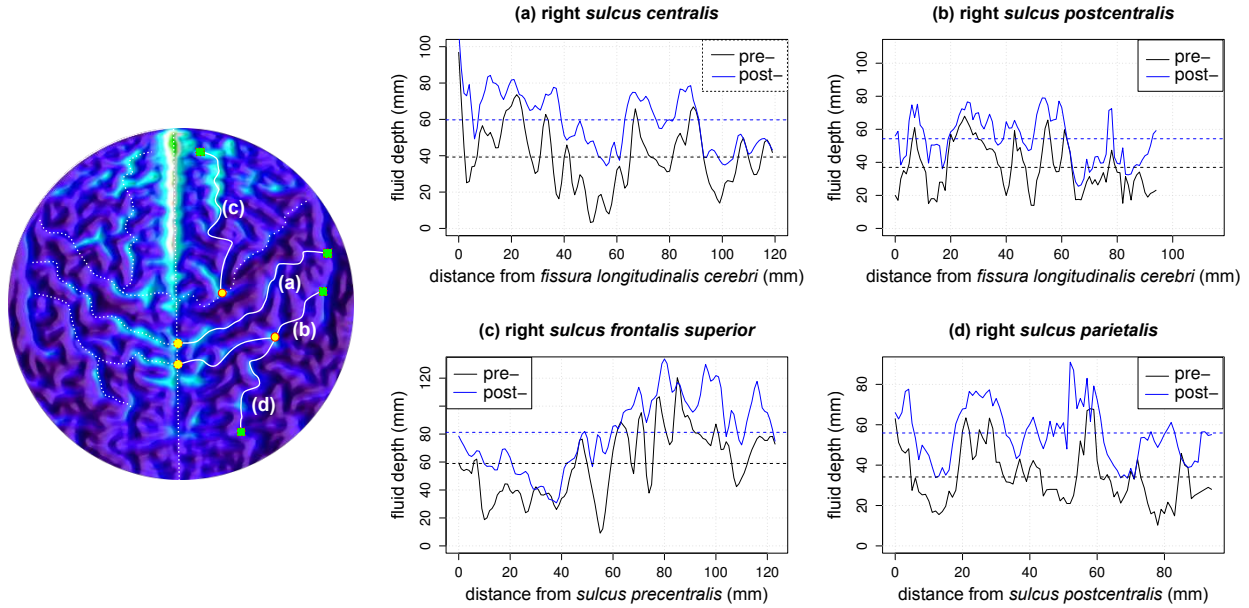
Figure 9: Examples of the fluid distribution depths along some cerebral sulci for a communicating hydrocephalus patient before and after a surgery (Fig. 8). Considered cerebral sulci are: a right *sulcus centralis* (a), a right *sulcus precentralis* (b), a right *sulcus frontalis superior* (c) and a right *sulcus intraparietalis* (d), each of which is drawn as a white curve starting at an orange circle to a green square.

$$Sk_y \quad = \quad -0.0448d + 0.0005d^2.$$

From these models, we can conclude that asymmetry of fluid distribution increases with depletion in the posterior regions of the brain if the fluid is increasingly concentrated in the frontal part of the *fissura longitudinalis cerebri*.

In summary, the center of mass and the skewness, to a lesser extent, could be both relevant discriminant factors to distinguish between healthy adults and hydrocephalus patients.

5.3. Descriptive discriminant analysis

As seen in the previous section that the center of mass could be a relevant discriminant factor, we perform a descriptive discriminant analysis [23] on the clinical dataset using the coordinates of the 74 centers of mass as the input variables. The software package R was used for this analysis [24].

We consider two classes: healthy adults and pathological cases (containing communicating and non-communicating hydrocephalus cases). The result provided the Wilks'lambda, which was significant (= 0.2114), with the *p*-value of

Table 2: Means with standard deviations of the low order moment-based features calculated from volumetric relief maps for healthy adults and pathological cases, respectively.

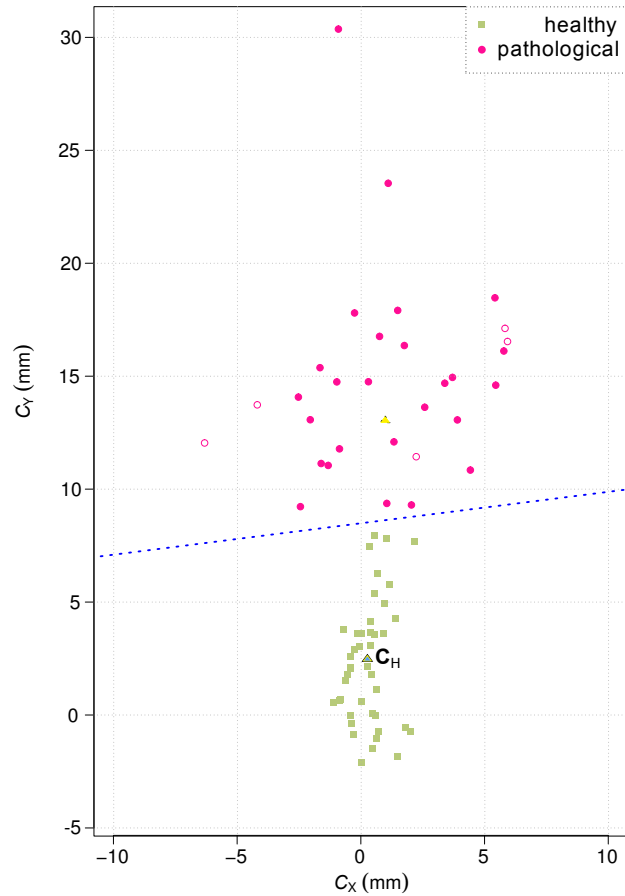| Moment order	Feature	Class	Value
0	volume (cm^3)	healthy	237 ± 51
		pathological	200 ± 83
1	center of mass (mm)	healthy	$C_x = 0.70 \pm 0.77$; $C_y = 2.33 \pm 2.70$
		pathological	$C_x = 0.91 \pm 2.71$; $C_y = 12.75 \pm 5.47$
2	orientation (degrees)	healthy	$\theta = 92 \pm 7$
		pathological	$\theta = 94 \pm 51$
3	skewness	healthy	$|Sk_x| = 0.03 \pm 0.02$; $Sk_y = -0.08 \pm 0.09$
		pathological	$|Sk_x| = 0.09 \pm 0.06$; $Sk_y = -0.42 \pm 0.21$

11

Figure 10: Distribution of the centers of mass for the clinical dataset with its descriptive discriminant analysis. The dotted line ($C_Y = 0.161C_X + 8.39$), resulting from the discriminant analysis in Section 5.3, indicates the limit values from which the centers of mass can be distinguished between healthy adults and hydrocephalus patients. Healthy adults have an average center of mass $\vec{C}_H$ close to the relief map center (bottom blue triangle). In contrast, hydrocephalus patients have fluid distributions depleted in the posterior region of the brain, with larger deviations around the *fissura longitudinalis cerebri* than healthy adults (the average is illustrated by the top yellow triangle; the centers of mass for non-communicating hydrocephalus patients are distinguished from those for communicating ones by red non-filled circles).
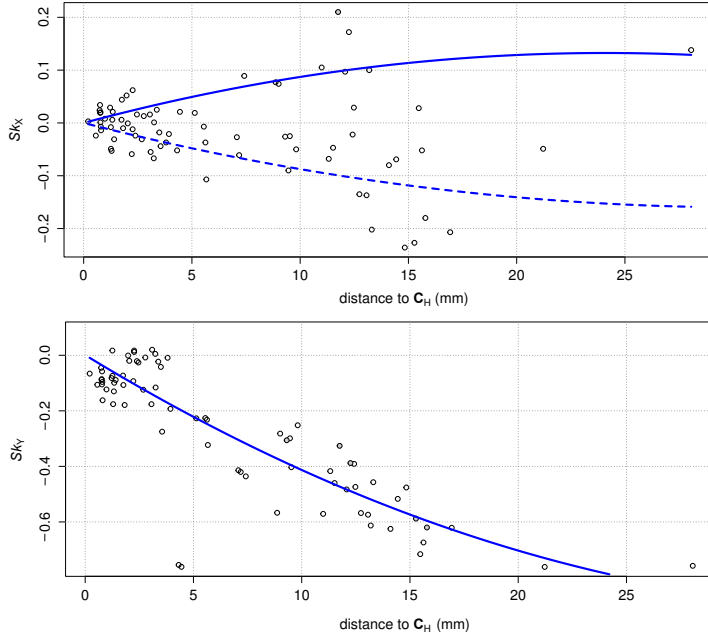
Figure 11: Evolution of the skewness coefficients Sk_x (top) and Sk_y (below) with respect to the distance d to the average center of mass for healthy adults $\vec{C}_H$. The quadratic regression between Sk_x and d gives: $Sk_x = -0.0113d + 0.0002d^2$ if $C_x > 0$ (in dashed line), $Sk_x = 0.0134d - 0.0002d^2$ if $C_x < 0$ (in solid line), and the one between Sk_y and d gives: $Sk_y = -0.0448d + 0.0005d^2$.

$2.2e - 16$. Thus, with a significance level of 0.001, this test indicated that the coordinates of centers of mass differentiated between healthy adults and pathological cases.

Let TP, FP, TN and FN be the respective numbers of true positives, false positives, true negatives and false negatives. The sensitivity S_e and the specificity (or recall) S_p are respectively defined as $S_e = TP/(TP + FN)$ and $S_p = TN/(TN + FP)$. The additional F_1-score metric, which is defined by $F_1 = 2pS_e/(p + S_e)$ where p stands for the precision, defined by $p = TP/(TP + FP)$, is also used to validate the classifier. For a training-testing ratio chosen to be two-thirds to one-third, the distinction between pathological cases and healthy adults results in 100% for all of the sensitivity S_e, the specificity S_p and the F_1-score. This analysis is efficient to discriminate between the above two classes. However, it still remains to be confirmed with a larger number of data. Figure 10 illustrates a result of the linear discriminant analysis with respect to the distribution of centers of mass.

5.4. Monitoring of patients

Volumetric relief maps can also be used to monitor patients before and after surgery. Figures 12 and 13 respectively show the distribution of centers of mass and the evolution of the skewness coefficients for eight patients who had magnetic resonance image acquisitions before and after their surgery. We observe that all patients after surgery have their centers of mass recovered to acceptable values, and that their skewness coefficients have decreased following the models presented in Section 5.2. The predicted classification between patients before and after surgery is performed by using the processed data in Section 5.3 as a training set for a linear discriminant analysis. This results in 100% for all of the sensitivity S_e, specificity S_p and F_1-score, and indicates its efficiency to discriminate between the classes and also to perform patient monitoring before and after surgery. Certainly, this still remains to be confirmed with a larger number of data.
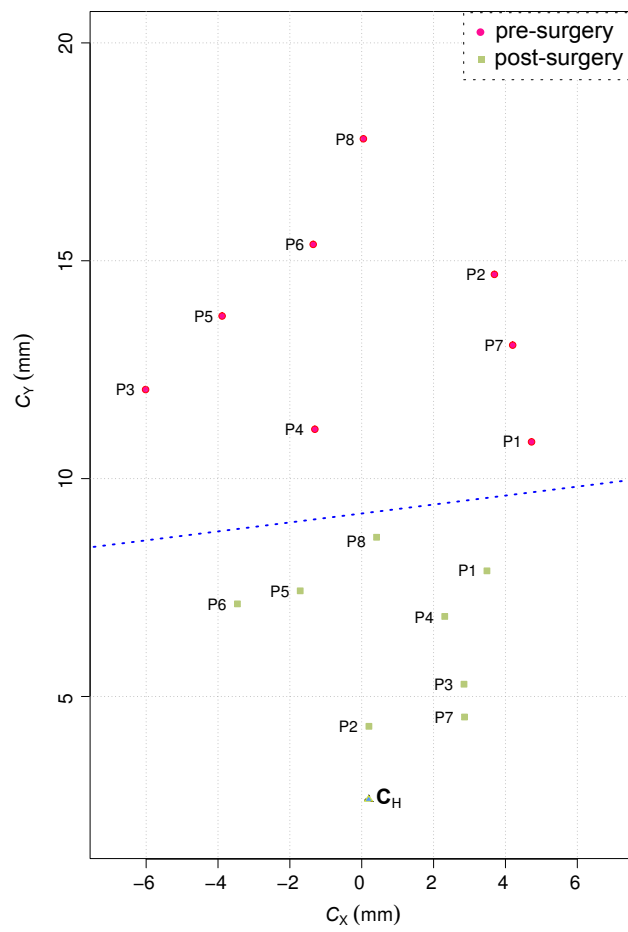
13

Figure 12: Monitoring of the centers of mass for pre- and post-surgery patients. The dotted line ($C_Y = 0.161C_X + 8.39$), resulting from the discriminant analysis, indicates the border by which the centers of mass for the two classes (healthy adults and patients) can be separated. It follows that each patient has recovered a normal state after the surgery.
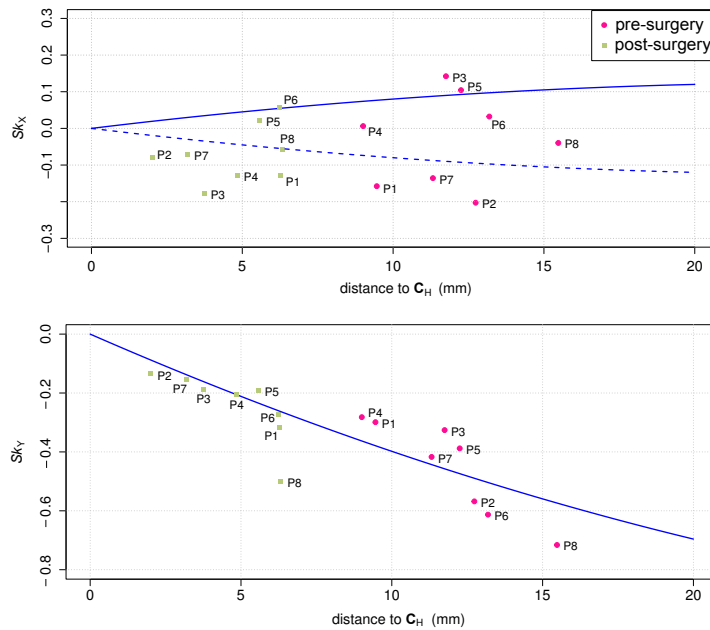
Figure 13: Monitoring of the skewness coefficients for pre- and post-surgery patients with the calculated evolution models in Fig. 11. Every patient has recovered a normal state after the surgery.

6. Conclusion

Given a pre-segmented magnetic resonance image of the cerebrospinal fluid within its cortical subarachnoid space, we presented a two-dimensional image representation of the fluid volume distribution called a volumetric relief map. Volumetric relief maps are automatically retrieved through ray-tracing and map-projection techniques from a volume data. They provide efficient representations that allow to visualize, at a glance, a complex structure such as the fluid volume distribution within the superior cortical subarachnoid space. We have also shown that fluid distributions are extracted from the maps and can be characterized using image moments in low orders. In particular, volumetric relief maps allow us to observe that fluid distributions are balanced for healthy adults, and also to compute their centers of mass that are close to the relief map center and their skewnesses hovering around zero. In contrast, hydrocephalus patients have fluid distributions depleted in the posterior region of their brain with various asymmetries. Such asymmetries increase with depletion, and are generally concentrated in the frontal part of the *fissura longitudinalis cerebri*. Indeed, the relative change of the averages of centers of mass between healthy adults and patients is −80% along the vertical axis of the map. These observations confirm that the above two moment-based features can be efficient discriminant factors to characterize and distinguish between healthy adults and pathological cases. Our tool also allows to monitor a variation of the cerebrospinal fluid distribution within the superior cortical subarachnoid space, before and after surgery, on a patient suffering from hydrocephalus. In future work, more precise analyses of various ways of evolution in pathological cases is expected; for example, decomposition of the fluid volume within sulci will be considered using a volumetric relief map.

References

[1] Sakka, L., Coll, G., Chazal, J.. Anatomy and physiology of cerebrospinal fluid. European Annals of Otorhinolaryngology, Head and Neck Diseases 2011;128(6):309–316.

[2] Rekate, H.L., Nadkarni, T.D., Wallace, D.. The importance of the cortical subarachnoid space in understanding hydrocephalus. Journal of Neurosurgery: Pediatrics 2008;2(1):1–11. doi:\bibinfo{doi}{10.3171/PED/2008/2/7/001}.

[3] Andriole, K.P., Wolfe, J.M., Khorasani, R., Treves, S., Getty, D.J., Jacobson, F.L., et al. Optimizing analysis, visualization, and navigation of large image data sets: One 5000-section CT scan can ruin your whole day. Radiology 2011;259(2):346–362.

[4] Lebret, A., Kenmochi, Y., Hodel, J., Rahmouni, A., Decq, P., Petit, E.. Relief map of the upper cortical subarachnoid space. In: CARS 2013. Computer Assisted Radiology and Surgery. Proceedings of the 27th International Congress and Exhibition, Heidelberg, Germany, June 26–29, 2013; vol. 8(Suppl 1). Heidelberg: Springer; 2013, p. S282–S284.

[5] Holländer, I.. Cerebral cartography – a method for visualizing cortical structures. Computerized Medical Imaging and Graphics 1995;19(5):397–415.

[6] Hurdal, M.K., Stephenson, K., Bowers, P., Sumners, D., Rottenberg, D.A.. Coordinate systems for conformal cerebellar flat maps. NeuroImage 2000;11(5):S467.

[7] Rettmann, M.E., Tosun, D., Tao, X., Resnick, S.M., Prince, J.L.. Program for assisted labeling of sulcal regions (PALS): Description and reliability. NeuroImage 2005;24(2):398–416.

[8] Tosun, D., Rettmann, M.E., Han, X., Tao, X., Xu, C., Resnick, S.M., et al. Cortical surface segmentation and mapping. NeuroImage 2004;23(Suppl. 1):S108–S118.

[9] Foley, J.D., van Dam, A., Feiner, S.K., Hughes, J.F.. Computer graphics: Principles and practice in C. Reading, MA: Addison-Wesley; 2nd ed.; 1995. ISBN 978-0-2018-4840-3.

[10] Bugaevskij, L.M., Snyder, J.. Map projections: A reference manual. London: Taylor & Francis; 1995. ISBN 978-0-7484-0304-2.

[11] Lebret, A., Hodel, J., Rahmouni, A., Decq, P., Petit, E.. Cerebrospinal fluid volume analysis for hydrocephalus diagnosis and clinical research. Computerized Medical Imaging and Graphics 2013;37(3):224–233. doi:\bibinfo{doi}{10.1016/j.compmedimag.2013.03.005}.

[12] Hodel, J., Silvera, J., Bekaert, O., Rahmouni, A., Bastuji-Garin, S., Vignaud, A., et al. Intracranial cerebrospinal fluid spaces imaging using a pulse-triggered three-dimensional turbo spin echo MR sequence with variable flip-angle distribution. European Radiology 2011;21(2):402–410.

[13] Erlich, S.S., Apuzzo, M.L.J.. The pineal gland: anatomy, physiology, and clinical significance. Journal of Neurosurgery 1985;63(3):321–341.

[14] Kimerling, A., Overton, W., White, D.. Statistical comparison of map projection distorsions within irregular areas. Cartography and Geographic Information Systems 1995;22(3):205–221.

[15] Klette, R., Rosenfeld, A.. Digital geometry: Geometric methods for digital picture analysis. San Francisco: Morgan Kaufmann; 2004. ISBN 978-1-5586-0861-0.

[16] Frangi, A.F., Niessen, W.J., Vincken, K.L., Viergever, M.A.. Multiscale vessel enhancement filtering. In: Wells, W., Colchester, A., Delp, S., editors. Proceedings of the 1st International Conference on Medical Image Computing and Computer-Assisted Intervention (MICCAI '98), Cambridge, MA, USA, October 11–13, 1998; vol. 1496 of *Lecture Notes in Computer Science*. Heidelberg: Springer-Verlag; 1998, p. 130–137.

[17] Vincent, L.. Morphological grayscale reconstruction in image analysis: Applications and efficient algorithms. IEEE Transactions on Image Processing 1993;2(2):176–201.

[18] Schindelin, J., Arganda-Carreras, I., Frise, E., Kaynig, V., Longair, M., Pietzsch, T., et al. Fiji: an open-source platform for biological-image analysis. Nature Methods 2012;9(7):676–682.

[19] Tao, X., Han, X., Rettmann, M.E., Prince, J.L., Davatzikos, C.. Statistical study on cortical sulci of human brains. In: Proceedings of the 17th International Conference on Information Processing in Medical Imaging (IPMI 2001), Davis, CA, USA, June 18–22, 2001; vol. 2082 of *Lecture Notes in Computer Science*. Heidelberg: Springer-Verlag; 2001, p. 475–487.

[20] Yun, H., Im, K., Yang, J.J., Yoon, U., Lee, J.M.. Automated sulcal depth measurement on cortical surface reflecting geometrical properties of sulci. PLoS ONE 2013;8(2):e55977. doi:\bibinfo{doi}{10.1371/journal.pone.0055977}.

[21] Flusser, J., Suk, T., Zitová, B.. Moments and moment invariants in pattern recognition. Chichester, West Sussex: John Wiley & Sons, Ltd; 2009. ISBN 978-0-4706-9987-4.

[22] Lafaye de Micheaux, P., Drouilhet, R., Liquet, B.. Le logiciel R. Statistique et probabilités appliquées; Paris: Springer-Verlag; 2011.

[23] Hastie, T., Tibshirani, R., Friedman, J.. The elements of statistical learning: Data mining, inference, and prediction. Springer Series in Statistics; New York: Springer; 5th ed.; 2009. ISBN 978-0-3878-4857-0.

[24] R Development Core Team, . R: A language and environment for statistical computing. R Foundation for Statistical Computing; Vienna; 2011. ISBN 3-900051-07-0.